DEVELOPMENTAL BIOLOGY

Heart neurons use clock genes to control myocyte proliferation

Emmanouil Tampakakis[1]*, Harshi Gangrade[1], Stephanie Glavaris[2], Myo Htet[1], Sean Murphy[1,3,4], Brian Leei Lin[1], Ting Liu[1], Amir Saberi[1], Matthew Miyamoto[1,3,4], William Kowalski[5], Yoh-Suke Mukouyama[5], Gabsang Lee[4,6], Liliana Minichiello[7], Chulan Kwon[1,3,4]*

Neurons can regulate the development, pathogenesis, and regeneration of target organs. However, the role of neurons during heart development and regeneration remains unclear. We genetically inhibited sympathetic innervation in vivo, which resulted in heart enlargement with an increase in cardiomyocyte number. Transcriptomic and protein analysis showed down-regulation of the two clock gene homologs *Period1/Period2 (Per1/Per2)* accompanied by up-regulation of cell cycle genes. *Per1/Per2* deletion increased heart size and cardiomyocyte proliferation, recapitulating sympathetic neuron–deficient hearts. Conversely, increasing sympathetic activity by norepinephrine treatment induced Per1/Per2 and suppressed cardiomyocyte proliferation. We further found that the two clock genes negatively regulate myocyte mitosis entry through the Wee1 kinase pathway. Our findings demonstrate a previously unknown link between cardiac neurons and clock genes in regulation of cardiomyocyte proliferation and heart size and provide mechanistic insights for developing neuromodulation strategies for cardiac regen5eration.

INTRODUCTION

The autonomic nervous system includes a sympathetic and a parasympathetic branch with opposing effects on heart rate, conduction velocity, contraction force, and relaxation (*1*–*4*). Increased activation of the sympathetic nervous system in adults is associated with a higher incidence of arrhythmogenesis, worsening heart failure, hypertension, and sudden cardiac death (*1*–*3*). In addition, incomplete sympathetic innervation of premature infants as documented by increased heart rate variability is associated with sudden infant death syndrome, increased incidence of coronary heart disease, hypertension, and changes in cardiac geometry and function (*5*–*7*). Nevertheless, the mechanistic contribution of sympathetic neurons (SNs) on cardiac maturation and its association with disease development in adult life remain largely understudied.

Postnatal cardiomyocyte maturation and withdrawal from cell cycle within the first week after birth account for the heart's limited ability to regenerate after injury (*8*–*10*). Therefore, there is pressing interest to identify ways with which to regenerate the heart (*8*, *11*). To this end, scientists have attempted to increase cardiomyocyte proliferation by manipulating cell cycle regulators (*11*–*15*). In support of this approach, more recent studies revealed that a higher number of preexisting cardiomyocytes or induction of cell cycle genes improves heart function after injury (*15*, *16*).

Previous research attempted to address the effect of sympathetic innervation on postnatal cardiomyocyte proliferation with conflicting results. Earlier studies suggested increased cell proliferation in sympathectomized animals, while later in vitro analyses supported the opposite effect (*17*, *18*). Notably, all previous studies either were done in vitro or used animal models of chemical sympathectomy, known to have nonspecific side effects on various neuronal cell populations (*19*). More recently, both chemical sympathectomy and vagal nerve resection, though physiologically opposite, were reported to regulate postnatal mouse heart regeneration after injury (*20*, *21*). Nevertheless, the precise effect of SNs on cardiomyocyte proliferation remains unknown. Our current study sought to examine the role of SNs on postnatal cardiac development. We demonstrate that sympathetic innervation decreases cardiomyocyte proliferation. Furthermore, we provide evidence that SNs induce clock genes that suppress the proliferation of postnatal cardiomyocytes by primarily regulating their entry into mitosis.

RESULTS

Sympathetic innervation inhibits postnatal cardiomyocyte proliferation

The mouse heart is innervated by SNs from midgestation [embryonic day 13.5 (E13.5)], and this continues throughout the postnatal stages (2 to 3 weeks) (*1*–*3*, *22*). During this period, developmental adjustments in cardiomyocyte function, morphology, and metabolism coincide with maturational changes of heart's SNs after birth (*23*, *24*). The primary regulator of cardiac sympathetic innervation is nerve growth factor (NGF), produced by smooth muscle cells of the epicardial coronary veins at E13.5. Then, the coronary arteries deeper within the developing myocardium (E15.5 to E17.5) mediate an epicardial to endocardial innervation gradient (*22*). Defective cardiac innervation does not result in vascular abnormalities (*22*). Global knockout of NGF causes lethality after birth (*25*), making it difficult to investigate the role of SNs in postnatal heart development. To avoid the early lethality, we conditionally deleted NGF in smooth muscle cells (Sm22a-Cre; NGF fl/−) and monitored SN innervation (fig. S1A). We first confirmed that Sm22a-Cre is expressed before

[1]Division of Cardiology, Department of Medicine, Johns Hopkins University, Baltimore, MD 21205, USA. [2]Division of Paediatric Oncology, Department of Paediatrics, Johns Hopkins University, Baltimore, MD 21205, USA. [3]Department of Biomedical Engineering, Department of Cell Biology, Cellular, and Molecular Medicine, Johns Hopkins University School of Medicine, Baltimore, MD 21205, USA. [4]Institute for Cell Engineering, Johns Hopkins University School of Medicine, Baltimore, MD 21205, USA. [5]Laboratory of Stem Cell and Neuro-Vascular Biology, Cell and Developmental Biology Center, National Heart, Lung, and Blood Institute, National Institutes of Health, Bethesda, MD 20892, USA. [6]Department of Neurology, Johns Hopkins University School of Medicine, Baltimore, MD 21205, USA. [7]Department of Pharmacology, Oxford University, Oxford, UK.
*Corresponding author. Email: etampak1@jhmi.edu (E.T.); ckwon13@jhmi.edu (C.K.)

cardiac innervation at E13.5 (fig. S1B) and then examined the degree of sympathetic innervation by performing whole-mount immunostaining of E18.5 and postnatal day 1 (P1) mice for tyrosine hydroxylase (TH), a marker of SNs. As compared to control hearts, the mutant hearts exhibited a profound suppression of SN innervation (Fig. 1, A and B), whereas immunostaining for acetylcholine transporter (AChT), a marker of parasympathetic neurons, showed uninterrupted parasympathetic innervation (fig. S1C). Similarly, immunofluorescence staining of cardiac sections of P7 mice showed the inhibition of SNs and the disturbance of the epicardial to endocardial innervation pattern in both atria and ventricles (Fig. 1C). We also confirmed that the total TH protein expression in hearts with disrupted SNs was profoundly suppressed (Fig. 1D). To verify the physiologic effect of suppressed sympathetic innervation, we performed conscious electrocardiographic recordings of early adult mice and confirmed that they had lower average heart rates and increased heart rate variability, indicating reduced sympathetic activity (Fig. 1, E and F, and fig. S1, D and E).

Within the first postnatal week, cardiomyocytes cease to proliferate and become hypertrophic and more binucleated (*8*, *10*, *23*, *24*). To examine whether sympathetic innervation affects the hyperplastic to hypertrophic transition of postnatal cardiomyocytes, we first analyzed the heart growth. Curiously, SN-deficient hearts (at P14) become larger in size (Fig. 1G). Next, we quantified the size and number of the resulting cardiomyocytes. Cardiomyocytes became smaller in size (Fig. 1H), whereas their total number was significantly increased in hearts lacking SNs (Fig. 1I). This suggests that SNs suppress cardiomyocyte hypertrophy and increase the number of cardiomyocytes in postnatal hearts. We subsequently analyzed the number of nuclei per cardiomyocyte and found that mutant hearts have a significantly higher percentage of mononuclear cardiomyocytes (Fig. 1J). This is consistent with previous reports where a higher number of cardiomyocytes are associated with more mononuclear cells (*8*, *16*). To test whether the higher number of myocytes is a result of increased proliferation, we performed immunofluorescence staining of dissociated postnatal cardiomyocytes and analyzed cells by flow cytometry. Curiously, SN-deficient hearts displayed a higher percentage of myocytes positive for Ki67, a marker of proliferation expressed throughout the cell cycle ($Ki67^+$; fig. S1, F and G). Further analysis showed increased percentages of cardiomyocytes positive for phosphohistone H3 (pH3) and 5-ethynyl-2′-deoxyuridine (EdU) (Fig. 1, K and L, and fig. S1, H and I). We also performed cell cycle analysis of isolated single cardiomyocytes from P7 SN inhibition (SNi) hearts and verified that a higher percentage of cells are in the S and mitosis phase, while a lower proportion are in G_0-G_1 phase (fig. S1J). Together, these data indicate that in the absence of SNs, more cardiomyocytes undergo DNA replication and enter mitosis, resulting in an increase in cell number and percentage of mononuclear myocytes.

Disruption of SNs up-regulates cell cycle genes and down-regulates clock genes in postnatal hearts

To gain mechanistic insights on the downstream pathways of cardiac SN signals, we performed RNA sequencing of postnatal hearts with suppressed SNs and littermate controls. Gene ontology (GO) and gene set enrichment analyses (GSEAs) showed the up-regulation of cell cycle, mitosis, and DNA replication genes in hearts with suppressed SNs (Fig. 2A and fig. S2A), supporting the observed phenotype. Genes regulating the circadian cycle were significantly down-regulated (Fig. 2A and fig. S2A). Furthermore, calcium handling, muscle contraction, and cardiomyopathy-related genes were decreased in hearts with suppressed sympathetic innervation, implying their potential role in functional maturation of cardiomyocytes (Fig. 2A and fig. S2A).

On the basis of our phenotypic and transcriptomic analysis, we decided to focus on how SNs regulate cardiomyocyte proliferation. To determine which phase of the cell cycle was affected, we examined the expression of the main cell cycle regulators. Notably, while expression of G_1 phase genes was unchanged, genes regulating the S phase and mitosis were significantly increased in hearts with inhibited SNs (Fig. 2B). Accordingly, several cytokinesis-related genes were also up-regulated (fig. S2B), but no significant difference was observed in the expression of cell cycle inhibitors (fig. S2C). These data indicate that SNs control cardiomyocyte proliferation by suppressing S phase and mitosis activators.

NGF does not affect cardiomyocyte proliferation

NGF is an antiapoptotic growth factor; therefore, its deletion is unlikely to cause increased cell proliferation (*4*, *20*). To exclude any confounding effect resulting from decreased NGF expression in the heart, we deleted NGF in $Mesp1^+$ cells—giving rise to all cardiac lineages—using the Mesp1-Cre driver. The deletion reduced SN innervation mildly (fig. S3A), which is likely due to the fact that a proportion of cardiac smooth muscle cells derive from neural crest cells ($Wnt\text{-}1^+$) (*26*, *27*) and not exclusively from $Mesp1^+$ cells. In addition, the heart size remained unchanged, and cell cycle and clock genes were not significantly affected by the deletion (fig. S3, B to D). Similarly, ex vivo treatment of neonatal mouse cardiomyocytes (NMCMs) with NGF did not affect cell cycle gene expression (fig. S3E). This suggests that the observed increased cardiomyocyte proliferation was not caused by reduced NGF expression.

Period1/*Period2* deletion increases cardiomyocyte proliferation

Several clock genes are known to couple with cell cycle genes in proliferating cells (*28*–*30*), and disruption of some clock genes has been linked to increased tumorigenesis (*31*, *32*) (*33*). On the basis of their down-regulation in SN-deficient hearts (Fig. 2A), we hypothesized that clock genes can affect cardiomyocyte proliferation. To test this, we first examined the expression of the main circadian cycle regulators in hearts harvested at random times during the day (*29*, *34*). Curiously, both *Period* homologs *Per1* and *Per2* were significantly down-regulated in mutant hearts (at P7 and P14), while *Bmal1* expression trended toward lower expression (Fig. 2C and fig. S4). This is consistent with GO/GSEA analysis and suggests that some of the clock genes may have a role in cardiomyocyte development. We subsequently verified the decreased Period1 (Per1) and Period2 (Per2) protein expression by Western blotting (Fig. 2D). Several calcium handling genes were also found down-regulated (Fig. 2E), suggesting that SNs affect functional development of cardiomyocytes as well. Down-regulation of Per1 and Per2 is linked to cell proliferation in several cell types, including tumors, fibroblasts, and osteoblasts (*33*, *35*–*37*). However, their roles have not been studied in the context of cardiomyocyte proliferation. To examine the specific effect of SNs on circadian gene expression patterns, we isolated P14 hearts from SNi and control mice at P14 at specific 4-hour intervals and analyzed the expression of the main circadian regulators. *Per1* and *Per2* as well as *Clock* gene oscillations were suppressed, while the

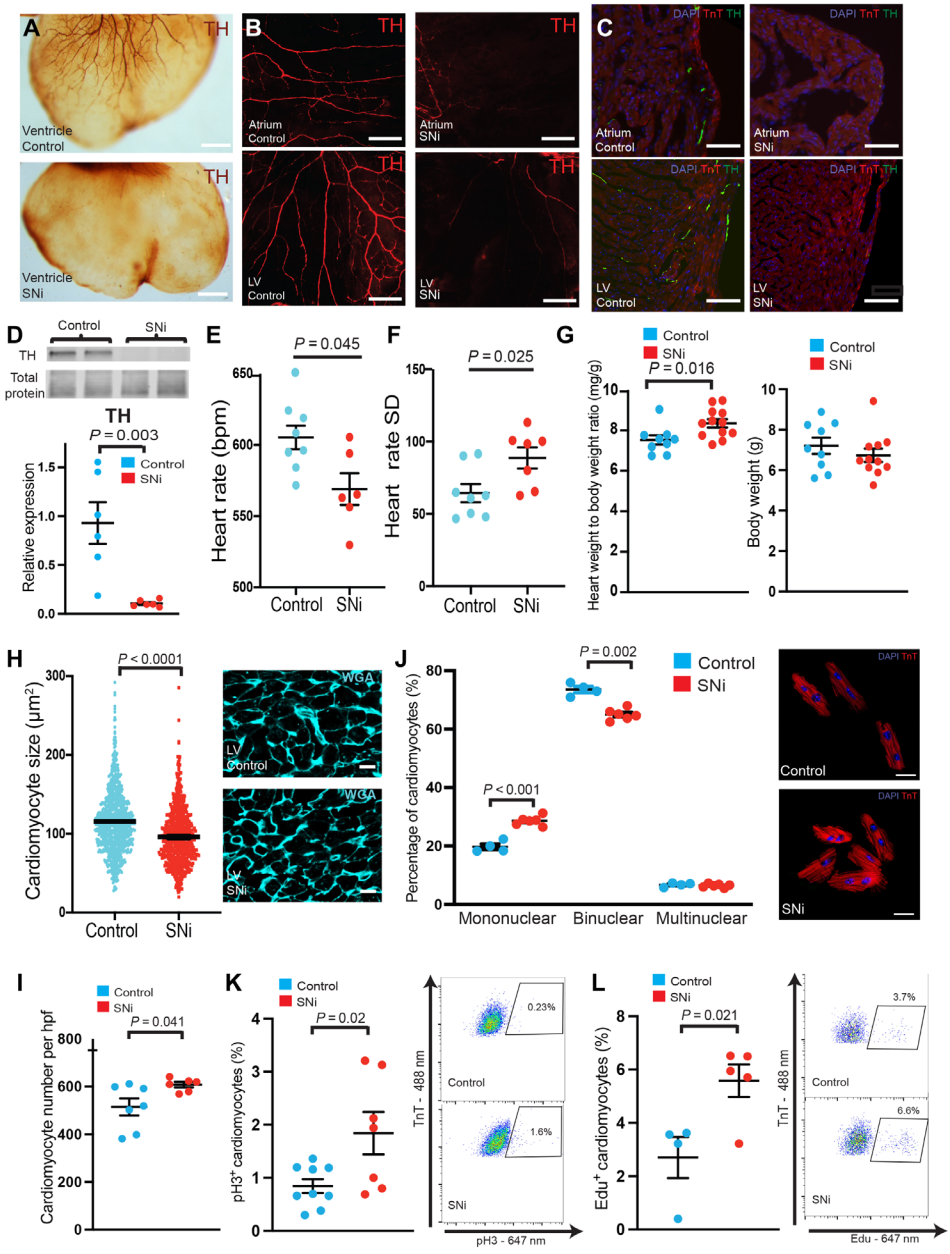

Fig. 1. Disruption of cardiac sympathetic innervation increases postnatal cardiomyocyte proliferation. (**A**) Whole-mount immunostaining of E18.5 mouse hearts for TH showing inhibition of sympathetic innervation (SNi) in mutant (Sm22a-Cre; NGF fl/−) hearts versus controls (NGF fl/+). Scale bar, 250 μm. (**B**) Whole-mount immunofluorescence staining of P1 mouse atria and left ventricle (LV) showing persistently reduced epicardial sympathetic innervation. Scale bar, 100 μm. (**C**) Immunostaining of P7 mouse hearts showing suppression of the epicardial to endocardial sympathetic innervation in the mutant heart atrium and left ventricle. Scale bars, 100 μm. (**D**) TH protein expression is profoundly reduced in hearts with suppressed sympathetic innervation. (**E**) Conscious mouse electrocardiographic recordings showing decreased average heart rates in mice with disrupted cardiac sympathetic innervation. (**F**) Mutant mice developed increased heart rate SD, consistent with increased heart rate variability. (**G**) Inhibited sympathetic innervation increased heart size, whereas body weight remained unchanged in mutant mice. (**H**) Cardiomyocytes with inhibited sympathetic innervation were smaller. Scale bars, 10 μm. (**I**) The total number of dissociated cardiomyocytes per high-power field (hpf) was increased in hearts with inhibited SNs. (**J**) Cardiomyocytes isolated from hearts with suppressed sympathetic innervation were more mononucleated and less binucleated. (**K** and **L**) Higher percentage of isolated P7 cardiomyocytes in hearts with suppressed sympathetic innervation were $pH3^+$ and EdU^+ as analyzed by flow cytometry. Student's *t* test was used for two-group analysis. Data are presented as means ± SEM. SNi, sympathetic neuron inhibition; TnT, troponin T. Photo credit: E. Tampakakis (The Johns Hopkins School of Medicine).

other regulators do not appear to be consistently affected by the lack of SN innervation (fig. S5). To test whether *Per1*/*Per2* affect heart development, we generated Per1/Per2 double knockout (DKO) mice. We first examined the effect of period proteins on cardiac sympathetic innervation and found that it was not affected (fig. S6A). Curiously, the size of Per1/Per2 DKO mouse hearts was increased at P14, and cardiomyocyte cell size was decreased (Fig. 3, A and B). Subsequent analysis showed that the total number of cardiomyocytes was increased

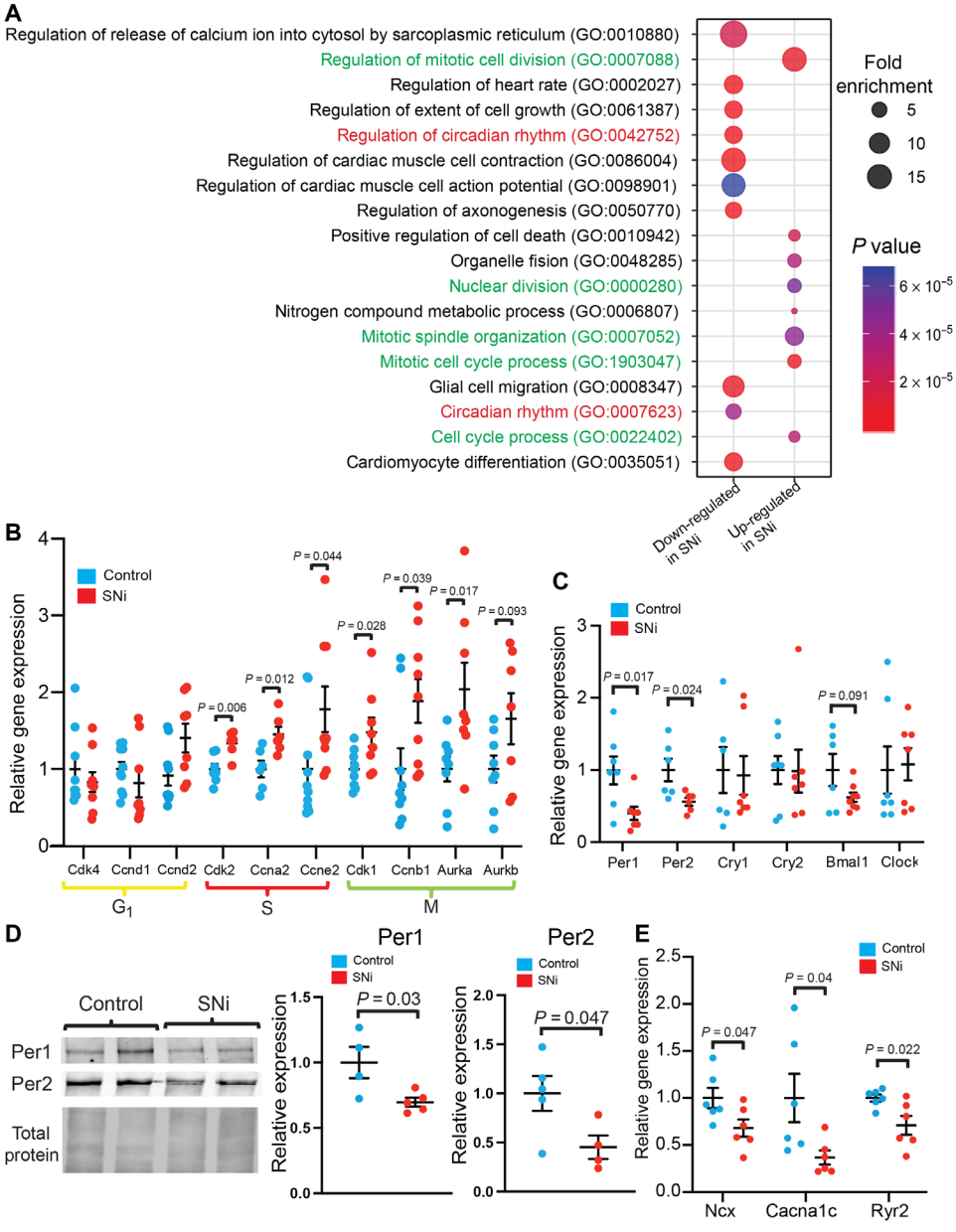

Fig. 2. Inhibition of cardiac SNs results in up-regulation of cell cycle genes and down-regulation of Per1 and Per2 genes. (**A**) GO analysis of RNA-sequencing data of P7 ventricles with disrupted sympathetic innervation compared to controls. Cell cycle, mitosis, and nuclear division genes were up-regulated (red), while circadian rhythm genes (green), calcium handling, cell size, muscle contraction, muscle action potential, heart rate, and axonogenesis genes were down-regulated. (All hearts were isolated at the same time, ~2 p.m.) (**B**) Quantitative PCR analysis of cell cycle regulators showing increased expression of genes regulating S phase and mitosis (M). (**C**) Gene expression analysis of circadian genes, showing decreased expression of *Per1* and *Per2* circadian cycle regulators. (**D**) Per1 and Per2 proteins were significantly reduced in hearts with suppressed sympathetic innervation. (**E**) Calcium handling genes were decreased in hearts with disrupted sympathetic innervation. Student's *t* test was used for two-group analysis. Data are presented as means ± SEM. Only *P* values <0.1 are reported.

in Per1/Per2 DKO mouse hearts (Fig. 3C), and there was a moderate but significant increase in the percentage of mononuclear cardiomyocytes (Fig. 3D). Moreover, Per1/Per2 DKO resulted in increased percentages of cardiomyocytes positive for Ki67, EdU, and pH3, suggesting that more cells are undergoing DNA replication and entering mitosis (Fig. 3, E and F, and fig. S5B). Cell cycle analysis also showed that a higher percentage of Per1/Per DKO cardiomyocytes were in the S and mitosis phase, while a smaller percentage of cells remained in G_0-G_1 phase (fig. S6C). This was further supported by increased expression of primarily mitosis-related genes in Per1/Per2 DKO hearts (Fig. 3G). Similar to the hearts with inhibited SNs, calcium handling genes were decreased (fig. S6D). In addition, cell cycle inhibitors remained unchanged, and cytokinesis-related genes were up-regulated (fig. S6, E and F). Together, these data suggest that *Period* genes negatively regulate postnatal cardiomyocyte proliferation.

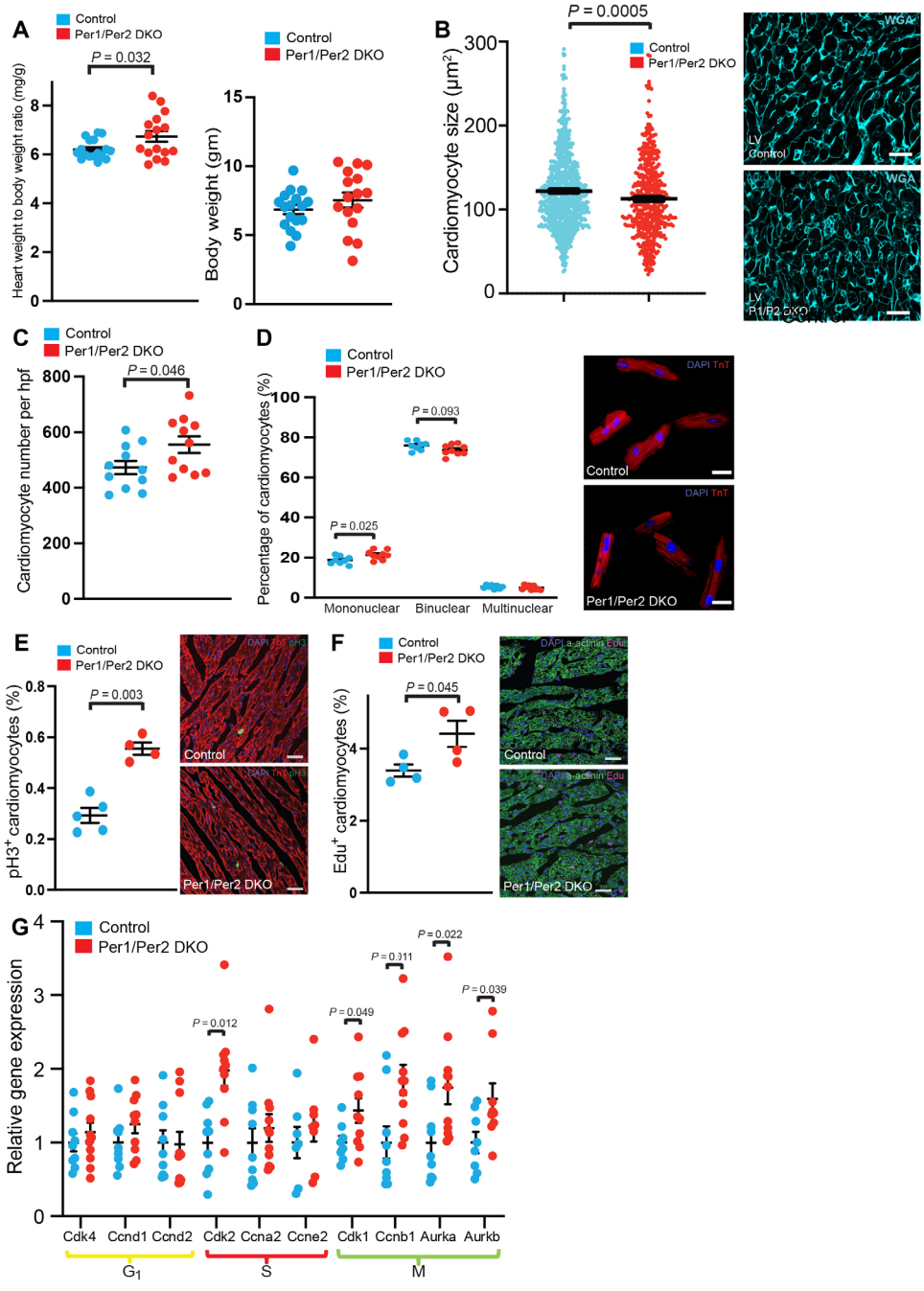

Fig. 3. Per1/Per2 DKO hearts have more proliferative neonatal cardiomyocytes. (**A**) Per1/Per2 DKO mice developed increased heart size, whereas total body weight remained unchanged at P14. (**B**) The size of individual Per1/Per2 DKO cardiomyocytes was decreased. (**C**) The total number of cardiomyocytes in Per1/Per2 DKO hearts was increased. (**D**) Per1/Per2 DKO myocytes were more mononucleated at P14. Scale bars, 20 μm. (**E**) Immunofluorescence staining of P7 cardiac sections for pH3 showed more Per1/Per2 DKO cardiomyocytes entering mitosis. Scale bars, 25 μm. (**F**) Immunofluorescence staining of P7 cardiac sections for EdU showed more Per1/Per2 DKO cardiomyocytes in the S phase. Scale bars, 25 μm. (**G**) Gene expression analysis of the major cell cycle regulators showed increased expression of genes regulating mitosis. Student's *t* test was used for two-group analysis. Data are presented as means ± SEM. Only *P* values <0.1 are reported.

Norepinephrine induces clock genes to suppress mitosis entry in cardiomyocytes

Adrenergic stimulation is known to induce clock gene expression in myocytes and liver cells (*38*, *39*), and *Per1/Per2* promoters contain cyclic adenosine 3′,5′-monophosphate (cAMP) response elements (CREs) (*34*, *40*). Commonly, adrenergic activation of G protein–coupled receptors activates adenylyl cyclase to increase cAMP, which stimulates protein kinase A and then cAMP-responsive element–binding protein (*41*). Because norepinephrine is the main postganglionic adrenergic neurotransmitter released by SNs, we hypothesized that

norepinephrine activation of G protein–coupled receptors and increased cAMP levels induce *Per1* and *Per2*. To test this, we first measured the norepinephrine concentration and verified that norepinephrine levels were profoundly suppressed in hearts with disrupted SNs, possibly accounting for the reduced *Per1* and *Per2* expression (Fig. 4A). We next cultured ex vivo NMCMs and first reset their cyclic expression by exposing them to 50% serum (fig. S7) (*42*). Then, we treated the cells with norepinephrine and examined the expression of clock genes after 48 hours. We found that the treatment induced *Per1* and *Per2* as well as *Cryptochrome1* (*Cry1*) and *Cry2* genes (Fig. 4B). We further examined whether norepinephrine could decrease cell cycle genes in NMCMs. Consistent with our in vivo data, norepinephrine suppressed mitosis genes (Fig. 4C). However, in the absence of Per1/Per2, there was no significant effect on cell cycle genes apart from *Aurkb* (Fig. 4C). This suggests that Per1 and Per2 are necessary for the norepinephrine-mediated suppression of mitosis.

Wee1 kinase is suppressed in SN-deficient and Per1/Per2-deleted hearts, leading to increased mitosis entry

To examine what factors might be regulating cardiomyocyte proliferation and mitosis entry downstream of Per1/Per2, we analyzed the expression of genes that are known to function as potential coupling factors between circadian and cell cycle factors (Fig. 5A) (*28*, *29*, *35*).

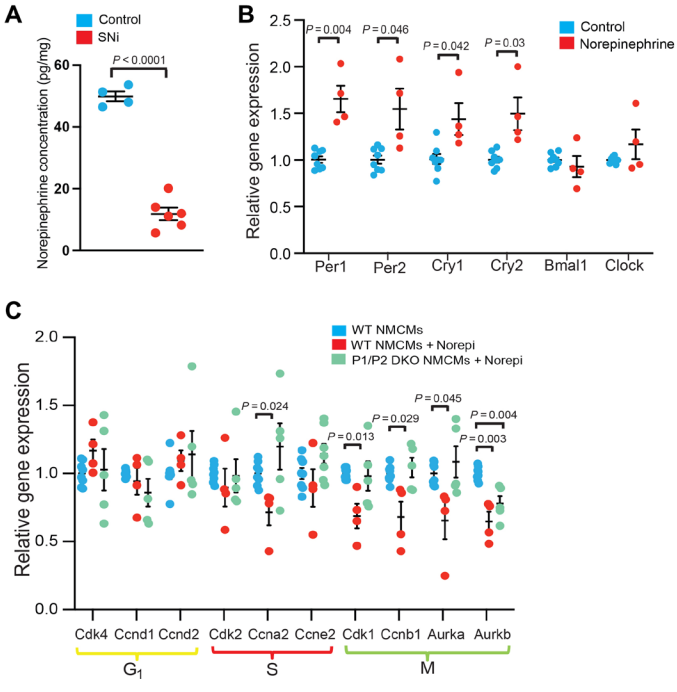

Fig. 4. Norepinephrine induces clock genes and suppresses cell cycle genes in NMCMs. (**A**) Norepinephrine concentration in heart with disrupted sympathetic innervation (SNi) is profoundly suppressed. (**B**) Norepinephrine induces the expression of circadian genes in wild-type NMCMs after 48 hours of treatment. (**C**) Norepinephrine decreased the expression of mitosis-regulating genes in wild-type NMCMs. Norepinephrine failed to suppress mitosis-regulating genes apart from *Aurkb* in cardiomyocytes isolated from Per1/Per2 DKO neonatal mouse hearts. Student's *t* test was used for two-group analysis. ANOVA test was used for multiple group comparisons. Data are presented as means ± SEM. Only *P* values <0.1 are reported.

Of all the genes tested, *Wee1*—a protein kinase that inactivates Cdk1 by phosphorylation at Tyr^{15}—was consistently down-regulated in hearts lacking Per1/Per2 and SNs (Fig. 5B). Contrarily, *Cdc25*—a phosphatase with the opposite effect of Wee1—was found increased in SNi hearts (Fig. 5B). We then verified that Wee1 protein was decreased in hearts lacking SNs or Per1/Per2 (Fig. 5, C and D). This suggests that the clock genes may use Wee1 to regulate mitosis entry in cardiomyocytes. To test this, we checked the levels of Cdk1/cyclin B1, a protein complex for mitosis entry whose activity is regulated by Wee1 via phosphorylation (Fig. 5A) (*15*, *43*). Both mutant hearts showed decreased levels of inactive phospho-Cdk1 (Tyr^{15}) and increased levels of active Cdk1 and cyclin B1 (Fig. 5, C and D). This suggests that decreased Wee1 expression is associated with higher levels of unphosphorylated and active Cdk1/cyclin B1 complex, resulting in a higher percentage of cardiomyocytes proliferating and entering mitosis. As Wee1 can also phosphorylate Cdk2 at the tyrosine-15 residue to inhibit cell cycle progression, we analyzed the regulation of Cdk2. Consistent with the gene expression, Cdk2 protein levels were increased; however, the levels of inactive phospho-Cdk2 (Tyr^{15}) remained decreased (fig. S8A). This suggests that similarly to Cdk1, reduced Wee1 expression can increase the transition to G_2-M phase through higher levels of unphosphorylated and active Cdk2. Last, we confirmed that norepinephrine induces Wee1 expression in NMCMs, but this effect was not observed in the absence of Per1/Per2 (Fig. 5E). This highlights that Wee1 regulates mitosis entry downstream of norepinephrine induction of Per1 and Per2. Period proteins were also shown to act as cell cycle suppressors through the regulation of DNA damage response and activation of p53 and ataxia telangiectasia mutated (ATM) (*29*, *44*). Nonetheless, we did not detect any difference in p53 and cell cycle inhibitors in both mutant hearts (Fig. 5B). In addition, there was no difference in levels of phospho-ATM (Ser^{1981}, active form) in either mouse models (fig. S8B).

Postnatal cardiomyocytes rapidly switch from anaerobic glycolysis to oxidative metabolism through increase in fatty acid oxidation and mitochondrial Krebs cycle. This results in the production of reactive oxygen species and reduced cardiomyocyte proliferation primarily through DNA damage response–mediated apoptosis (*45*). To examine whether suppressed cardiac sympathetic innervation or deletion of Per1/Per2 affects oxygen consumption rate (OCR), we performed Seahorse analysis in isolated postnatal (P14 to P18) cardiomyocytes. Basal OCR and adenosine 5′-triphosphate (ATP) synthesis in SNi cardiomyocytes were reduced, while there was no significant difference in glycolysis [extracellular acidification rate (ECAR) to OCR ratio] (fig. S9, A to E). In contrast, Per1/Per2 cardiomyocytes did not show significant changes in oxidative metabolism (fig. S9, F to J). This suggests that in SNi hearts, reduced oxidative metabolism may also influence increased cardiomyocyte proliferation.

Period2 binds to Wee1 promoter

An earlier liver study showed that Per1 and Per2 bind to the *Wee1* locus (*46*). To examine whether Per is physically associated with the *Wee1* promoter in postnatal hearts, we performed chromatin immunoprecipitation (ChIP) with Per2 antibody followed by quantitative polymerase chain reaction (qPCR) analysis. We found enrichment of two regions within the *Wee1* promoter (proximal and distal) bound by Per2, suggesting that Per2 may directly regulate *Wee1* expression (Fig. 6A) (*46*). To test this, we constructed luciferase reporter plasmids containing the intact Wee1 promoter with/without the proximal or distal Per2 binding site and subsequently analyzed

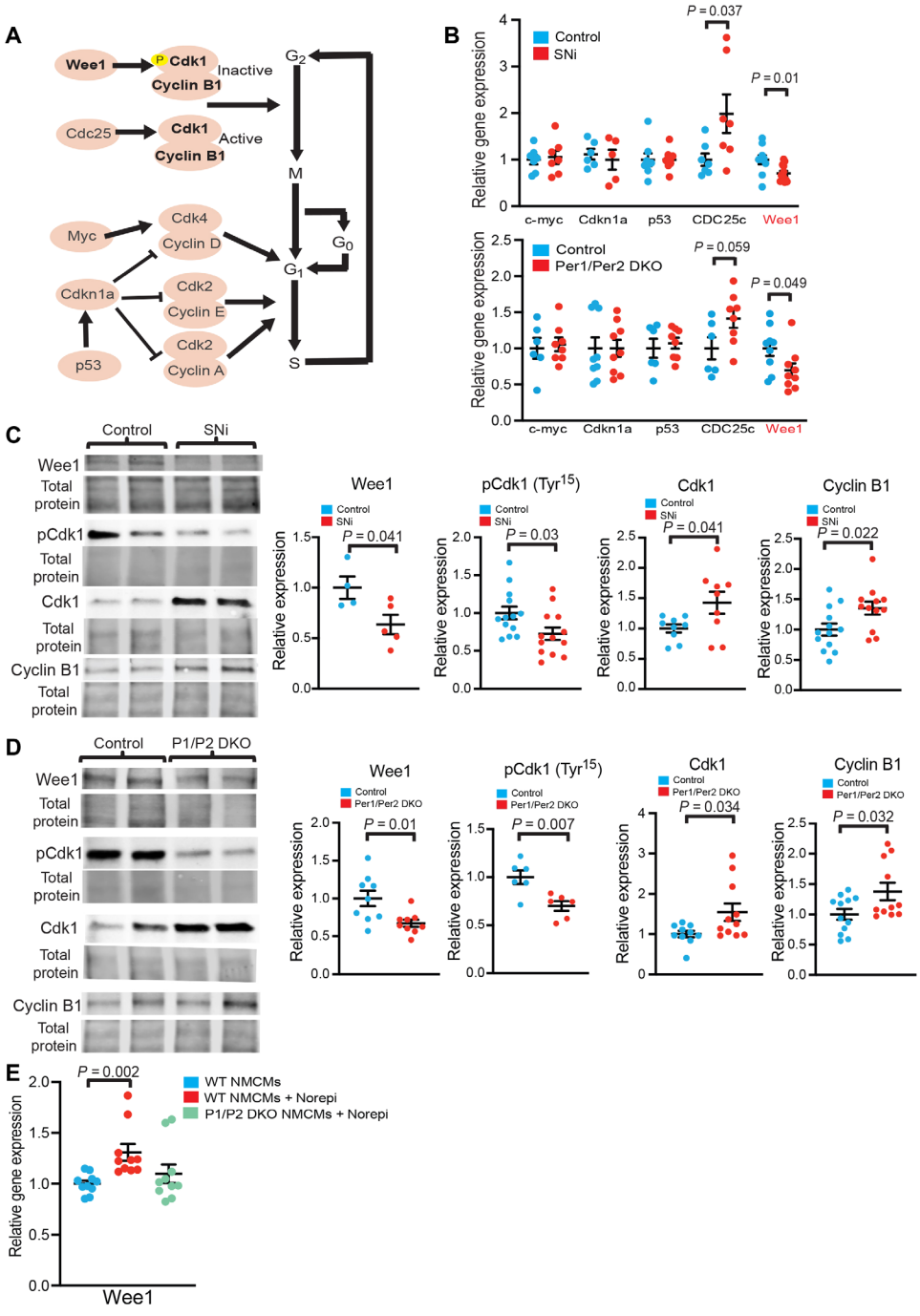

Fig. 5. In hearts with disrupted sympathetic cardiac innervation and in Per1/Per2 DKO hearts, suppression of Wee1 kinase activates the Cdk1/cyclin B1 mitosis entry complex. (**A**) Schematic representation of the different proteins linking the cell cycle with the circadian cycle. Wee1 is a kinase that phosphorylates and inactivates Cdk1, not allowing the Cdk1/cyclin B1 complex to induce entry into mitosis. Cdc25 is a phosphatase with the opposite effect. (**B**) Gene expression analysis of factors known to link Per1/Per2 and cell cycle showed that *Wee1* is consistently decreased in both hearts with inhibited sympathetic innervation and Per1/Per2 DKO. *Cdc25* is significantly increased in SNi hearts. (**C** and **D**) Western blot analysis confirmed decreased expression of Wee1 protein kinase and increased expression of Cdk1 and cyclin B1 proteins in hearts with disrupted sympathetic innervation and Per1/Per2 DKO. Phosphorylated Tyr^{15} Cdk1 was decreased in both mouse models suggestive of increased Cdk1 activation. (**E**) Norepinephrine treatment of wild-type NMCMs induced *Wee1* gene expression; however, this effect was not observed in Per1/Per2 DKO cardiomyocytes. Student's *t* test was used for two-group analysis. ANOVA test was used for multiple group comparisons. Data are presented as means ± SEM. Only *P* values <0.1 are reported.

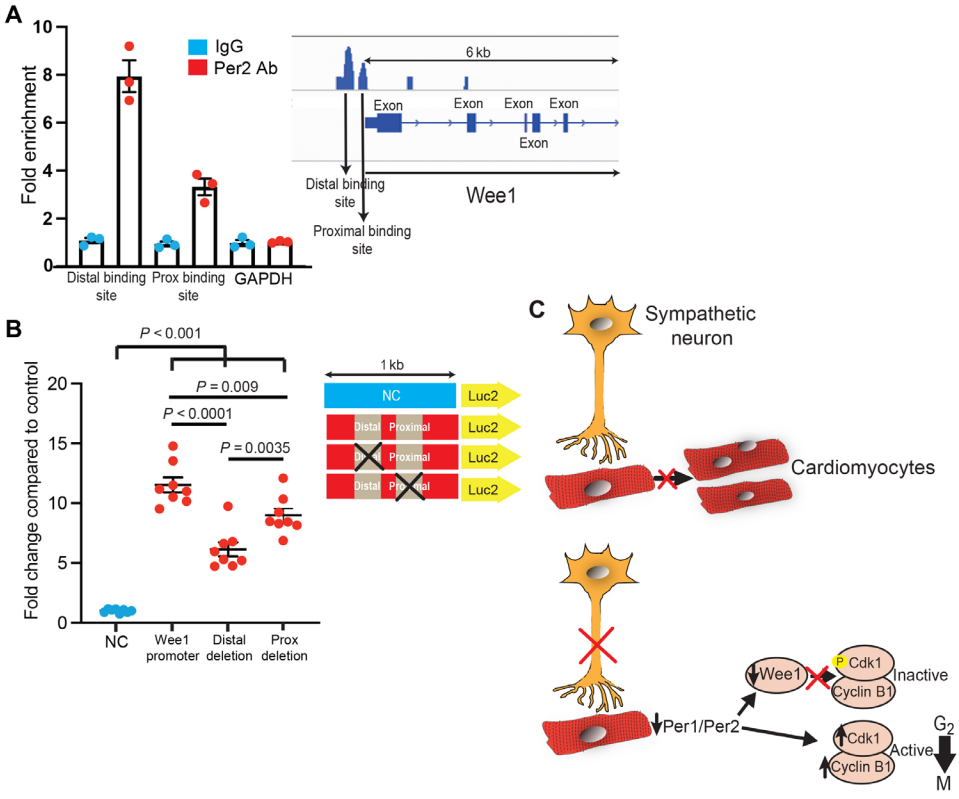

Fig. 6. Per2 binds Wee1 and Cdk1 to likely regulate their expression. (**A**) ChIP-qPCR analysis of P7 hearts using Per2 antibody (Ab) showing increased enrichment of two regions within the *Wee1* promoter in comparison to *GAPDH* control. IgG, immunoglobulin G. (**B**) Luciferase expression assay in human stem cell–derived cardiomyocytes. Intact Wee1 promoter resulted in increased luciferase activity. Deletion of either Per2 binding sites reduced luciferase activity, and the distal Per2 binding site had a more pronounced effect. NC, negative control. (**C**) Schematic representation of our working model.

the luciferase activity in cardiomyocytes derived from human pluripotent stem cells (PSCs). We found that both Per2 binding regions can increase luciferase activity, with the distal region having a more pronounced effect (Fig. 6B). This is consistent with the ChIP-qPCR data and suggests that these Per2 sites are important for *Wee1* expression. We also similarly found that Per2 can bind a previously described Cdk1 intronic region, suggesting that it may regulate Cdk1 expression as well (fig. S10).

DISCUSSION

Earlier studies using in vitro cell cocultures or rodent models of chemical sympathectomy reported that SNs can increase cardiomyocyte cell size and contractility, organize the sarcomeric structure, and regulate electrophysiological properties (*47*–*49*). However, the lack of a genetically modified animal model makes it difficult to assess the role of SNs in a more comprehensive and conclusive manner (*17*, *18*). While not cardiac specific, our genetic animal model demonstrates robust inhibition of cardiac SN innervation, enabling us to address the contrasting views of SN function and to elucidate downstream mechanisms underlying cardiomyocyte proliferation.

The effect of sympathetic innervation on postnatal cardiomyocyte proliferation has been rather unsettled (*17*, *18*). Previous research has mostly focused on β-adrenergic signaling, with data supporting both increased cardiomyocyte endowment and decreased proliferation (*16*, *50*). In our study, cardiomyocytes with disrupted SNs were smaller in size, which is in agreement with the hypertrophic effect of β-adrenergic signaling (*51*). Our work is also in line with a recent report by Liu *et al.* (*16*), where β-adrenergic receptor inhibition increased the total number and percentage of mononuclear cardiomyocytes. In that study, however, β-adrenergic signaling affected cytokinesis without increasing cardiomyocyte proliferation. We believe that this discrepancy is likely due to the different animal models and the pleiotropic effects of SNs on cardiomyocytes (*52*), which can also be mediated through α-adrenergic receptors.

Cyclin-dependent kinases and cyclins are synchronized, and their expression after P5 in mouse hearts is precipitously decreased, leading to cell cycle withdrawal (*53*). Increased levels of Cdk1/cyclin B1 or decreased Cdk1 phosphorylation at Tyr^{15} at P7 induces cardiomyocyte proliferation and entry to mitosis (*15*, *53*). Therefore, the balance between Wee1 and Cdc25 to regulate Cdk1 phosphorylation is critical for cardiomyocyte mitosis (*15*, *43*, *54*). Our data support the idea that decreased expression of both *Per1* and *Per2* clock genes increases cardiomyocyte proliferation and mitosis entry through suppression of Wee1.

The hypothalamic suprachiasmatic nucleus synchronizes all peripheral circadian clocks in different organs (*29*, *34*). Nevertheless, each organ maintains its own independent circadian cycle by a cell-autonomous transcriptional feedback loop, where Per1 or Per2 forms heterodimers with Cry1 or Cry2 and migrates to the nucleus to regulate the expression of several genes including *Bmal1* and *Clock*. In the heart, the number of oscillating genes increases over time, and

Per1 and Per2 are up-regulated postnatally (P3 to P5), with their expression progress concurrently with cardiac innervation (*42*, *55*). We demonstrated that SNs can directly regulate *Per1/Per2* oscillations in the heart predominantly through adrenergic signaling. Up-regulation of *Per1/Per2* genes in postnatal hearts is likely critical for the fine-tuning and synchronization of the circadian cycle (*56*, *57*). It is worth noting that our findings do not necessarily support the involvement of circadian rhythm in cardiomyocyte proliferation and rather suggest the presence of a circadian rhythm–independent role of Per1/Per2.

Early research supports the idea that Per1 can directly inhibit Cdk1 and cyclin B1 expression, and Clock/Bmal1 can induce Wee1 (*30*, *35*). Nevertheless, it appears that Wee1 regulation is more complex, as its promoter is subjected to chromatin remodeling and hyperacetylation (*58*). More recent studies report that Per1 and Per2 can directly induce Wee1 (*59*–*61*) and increase Bmal1 expression (*62*). Likewise, mathematical modeling of clock genes and cell cycle interaction predicts that in Per2 mutant cells, dysregulation of the circadian cycle will result in lower levels of Bmal1 and Wee1 and increased cell entry into mitosis (*33*, *63*). Therefore, lower Wee1 expression could be due to either relatively decreased Bmal1 levels or lack of direct induction by the Period proteins as documented by our ChIP analysis.

We acknowledge that our analysis has specific limitations. First, we were not able to study cardiac-specific Per1/Per2 deletion due to the unavailability of Per1/2 conditional KO animals. Nevertheless, given the immaturity of circadian cycle at neonatal stages, it is less likely that Per1/Per2 can alter the behavior of neonatal mice or that other organs indirectly affect cardiac physiology. Furthermore, while we investigated the effect of Per1/Per2 DKO based on our bioinformatics analysis and their redundant roles, we realize that Per1 and Per2 may not exclusively have overlapping roles. Although the role of the circadian rhythm on cardiomyocyte proliferation is an interesting topic, it would require further investigation. Last, while the present study aims to determine the effect of SN innervation on cardiomyocyte proliferation during postnatal heart development, we do not know whether SNs have similar roles in adult hearts. The suppression of Per1/Per2 does not solely account for the increased postnatal myocyte proliferation in SNi hearts. Reduced oxidative metabolism, as demonstrated by our oxygen consumption analysis, may also contribute to increased neonatal cardiomyocyte proliferation in SNi hearts. Furthermore, potential increased activation of the neuregulin or the Hippo pathway could account for additional effects (*8*). Follow-up studies would be necessary to address these limitations.

While the present study focused on the role and mechanisms of SNs regulating myocyte proliferation, growing evidence suggests that SNs also promote structural and functional maturation of cardiomyocytes (*49*, *64*). Recent transcriptomic studies suggested that significant levels of cardiomyocyte maturation occur after birth, accompanied with down-regulation of cell cycle regulators (*65*). Given that the immaturity of PSC-derived cardiomyocytes remains a major obstacle for modeling late-onset heart disease (*66*), elucidating the instructive role of SNs may help us develop new strategies to generate mature cardiomyocytes from PSCs. It is likely that various pathways apart from Per1/Per2 mediate the pleiotropic effects of SNs in cardiomyocytes as previously reported (*64*).

In summary, our study shows that SNs decrease postnatal cardiomyocyte proliferation. The lack of cardiac SNs suppresses *Per1/Per2* circadian proteins, which results in the up-regulation of Cdk1/cyclin B1 and the inhibition of Wee1 kinase that activates Cdk1 and ultimately increases cardiomyocyte proliferation and entry into mitosis (Fig. 6C). We believe that our study provides previously unknown insights into the role of cardiac sympathetic innervation in regulating clock and cell cycle genes in postnatal hearts.

MATERIALS AND METHODS

Animals

Sm22a-Cre (017491) and C57BL/6 mice were obtained from The Jackson Laboratory. $NGF^{+/-}$ mice were donated by C. Deppmann (*67*), NGF fl/fl mice were donated by L. Minichiello (*68*), and Per1/Per2 DKO mice were donated by J. Pendergast. Mesp1-Cre mice were generated by Saga *et al.* (*69*). All animals were housed at the Johns Hopkins Medical Institutions. The animals were randomly allocated to experimental groups, and both male and female mice were equally used in all experimental assays. All mouse hearts and cardiomyocytes were harvested at random times during the day unless specified otherwise.

Cardiomyocyte culture

Cardiomyocytes were isolated from P0 or P1 mouse hearts using a neonatal cardiomyocyte isolation kit (Miltenyi Biotec) based on the manufacturer's instructions. Before plating, cardiomyocytes were filtered through a 70-μm mesh, and single cells were cultured in 24-well plates coated with gelatin. The cells were first maintained in 5% fetal bovine serum (FBS) in Dulbecco's modified Eagle's medium (DMEM) with penicillin/streptomycin antibiotics for 24 hours and subsequently treated for at least 2 hours with 50% horse serum in DMEM and then for 2 days with 5% FBS in DMEM. Cardiomyocytes were treated with norepinephrine (1 μM) (Sigma-Aldrich) or NGF (10 ng/ml) (PeproTech) as indicated.

Luciferase assay

Human embryonic stem cells (hESC line H9, WiCell Research Institute) were used. hESCs were maintained and differentiated as done previously (*70*). Briefly, hESCs were maintained in essential 8 medium (Thermo Fisher Scientific), and they were sequentially treated with 6 μM CHIR99021 (Tocris, glycogen synthase kinase 3b inhibitor) for 48 hours followed by 2.5 μM IWR-1 (Tocris, Wnt signaling antagonist) in RPMI-B27 without insulin (Thermo Fisher Scientific). Spontaneous beating was noted at day 7 of differentiation. Cardiomyocytes were further selected using sodium lactate (100 mM) for 3 days. Then, cells were replated in gelatin-coated plates, and 24 hours later, they were transfected with the respective vectors using the Lipofectamine Stem reagent (Thermo Fisher Scientific). More specifically, we used a dual luciferase reporter assay system (Promega) and transfected cardiomyocytes with the modified luciferase vector (pGL4.10, Promega) and the Renilla luciferase vector (pGL4.70, Promega), which was used as internal control. Cardiomyocytes were lysed 2 days later following the manufacturer's instructions, and luciferase levels were measured using a GloMax luminescence plate reader (Promega).

Whole-mount immunostaining

Hearts from E18.5 mouse embryos were dissected, fixed in 4% paraformaldehyde, subsequently dehydrated by methanol series, and incubated overnight in 20% dimethyl sulfoxide/80% methanol solution

containing 3% H_2O_2. Hearts were then rehydrated, blocked overnight with 4% bovine serum albumin (BSA) in 1% phosphate-buffered saline–Tween 20 (PBS-T), and incubated for 48 to 72 hours with anti-TH antibody (Novus, NB300-109, 1:200), followed by incubation with horseradish peroxidase (HRP)–conjugated antibody (1:500, Abcam). The signal was detected using diaminobenzidine (Sigma-Aldrich). Hearts were refixed and dehydrated by methanol and cleared by benzyl benzoate/benzyl alcohol (2:1). Imaging was performed using a Zeiss stereoscopic microscope. For whole-mount immunofluorescence staining, pups were euthanized and fixed in 4% paraformaldehyde for 24 hours. Hearts were dissected and cut in half, blocked with 10% goat serum in PBS-T, and incubated overnight with anti-TH or anti-AChT antibodies. Then, hearts were stained with Alexa Fluor secondary antibody (594) (Life Technologies; 1:500), mounted, and imaged using an EVOS fl (AMG) microscope.

Immunohistochemistry

Hearts were fixed in 4% paraformaldehyde, then placed in 30% sucrose followed by optimal cutting temperature compound (OCT), and sectioned. For immunofluorescence staining, they were blocked for 1 hour with 1% BSA and incubated overnight with the following primary antibodies: α-actinin (Abcam, ab68167), troponin-T (Thermo Fisher Scientific, MS-295-P1), pH3 (Millipore, 05-806), Ki67 (Abcam, ab15580), and TH (Novus, NB300-109). Alexa Fluor secondary antibodies (488, 594, and 647) (Abcam, Life Technologies) were used for secondary detection, and 4′,6-diamidino-2-phenylindole (DAPI) was added for nuclei staining. To assess cardiomyocyte size, heart sections were stained with wheat germ agglutinin–Alexa Fluor 647 (W32466). Cells were imaged using a Leica SP8 confocal microscope. All imaging analysis was performed by two blinded investigators using ImageJ (version 1.52q).

Mouse electrocardiography

Electrocardiogram (ECG) recordings were performed using adult mice as previously described (*71*). Briefly, 6-week-old mice were anesthetized with 4% isoflurane, intubated, and placed on ventilator support. The animal's upper back was opened with a small midline incision, and ECG leads were implanted subcutaneously and sutured over the trapezius muscle on both sides. Body temperature was maintained at 37°C. Immediately following implantation, the wound was sutured. ECG was subsequently recorded continuously using the PowerLab data acquisition device and LabChart 8 software (AD instruments). Mice were kept at a stable temperature with regular 12-hour light/dark cycle. ECGs were recorded in conscious animals for approximately 7 days for each mouse. To exclude the effect of increased vagal nerve activation as a result of pain and anesthesia, ECG recordings after day 4 were exclusively analyzed. Heart rate variability analysis was performed using LabChart 8 following published guidelines (*72*). More specifically, the heart rates were averaged over 12 hours (daytime and nighttime separately), and six independent average values per animal (3 days of total recording) were analyzed.

Heart dissociation and flow cytometry

Harvested hearts were placed in a Langendorff system and perfused with a type 2 collagenase (Worthington) and protease (Sigma-Aldrich) digestion buffer. Whole hearts were then triturated until no residual undigested tissue and filtered through a mesh. Single cardiomyocytes were subsequently fixed with 4% paraformaldehyde for 1 hour and then washed with PBS. For flow cytometry, cells were permeabilized with saponin (Sigma-Aldrich) and stained with troponin T (Thermo Fisher Scientific, MS-295-P1) and either pH3 (Millipore, 05-806) or Ki67 (Abcam, ab15580), followed by incubation with Alexa Fluor secondary antibodies (488, 647) (Abcam). For EdU analysis, the Click-iT EdU Kit (Life Technologies) was used followed by immunostaining with primary and secondary antibodies. Cell cycle analysis was performed using cardiomyocytes isolated from P7 mice after staining with Hoechst 33342 (Invitrogen) and cardiac troponin T. Flow cytometry was performed using BD Accuri C6. Data were analyzed using FlowJo software (version 10.5). To examine cardiomyocyte number and nucleation, cells were similarly stained for troponin T and DAPI and imaged using EVOS fl (AMG). All samples were analyzed by two blinded investigators.

RNA sequencing

Hearts were dissected, washed in PBS, and homogenized in TRIzol (Thermo Fisher Scientific), and RNA was isolated following the manufacturer's instructions. All hearts for each time point were isolated at the same time (2 p.m. for P7 and 10 a.m. for P14). Complementary DNA (cDNA) libraries for bulk-RNA sequencing were prepared using the TruSeq Kit (Illumina) and sequenced using HiSeq 2500. Raw sequencing reads were trimmed using Trimmomatic (0.36) with a minimum quality threshold of 35 and minimum length of 36 (*73*). Processed reads were mapped to the mm10 reference genome using HISAT2 (2.0.4). Counts were then assembled using Subread featureCounts (1.5.2) in a custom bash script. Differential gene expression analysis was done using the DESeq2 package in R. GO analysis was performed using PANTHER. Canonical pathway analysis was done using Ingenuity Pathway Analysis (QIAGEN Inc.).

Quantitative PCR

RNA was isolated from mouse hearts and cultured cardiomyocytes using TRIzol, and cDNA was generated using the High-Capacity cDNA Reverse Transcription Kit (Applied Biosystems). qPCRs were performed using the SYBR Select qPCR Mix (Thermo Fisher Scientific) with indicated primers. Gene expression levels were normalized to *Gapdh* or *Rpl32*.

Western blotting

Protein sample preparation from mouse ventricles was performed with tissue homogenization in Cell Lysis buffer (Cell Signaling Technology) with added phenylmethylsulfonyl fluoride (Sigma-Aldrich) and PhosStop (Roche). Protein concentration was determined by bicinchoninic acid assay (Pierce). Electrophoresis was performed using 4 to 20% tris-glycine TGX gels (Bio-Rad), and proteins were transferred onto nitrocellulose membranes. The following primary antibodies were used for immunoblotting: TH (Novus, NB300-109, 1:1000), Per1 (BioLegend, 936002, 1:1000), Per2 (Abcam, Ab180655, 1:1000), Wee1 (Abcam, Ab137377, 1:1000), phospho-Cdk1 (Y15) (Cell Signaling, 9111T, 1:1000), Cdk1 (Novus, NBP2-67438, 1:1000), cyclin B1 (Santa Cruz Biotechnology, SC-245, 1:1000), phospho-ATM (S1982) (Santa Cruz Biotechnology, SC-47739, 1:1000), Cdk2 (Cell Signaling Technology, 2546S, 1:500), and phospho-Cdk2 (Y15) (Novus, NBP2-67686, 1:1000). IRDye secondary fluorescent-conjugated antibodies were used (Li-Cor, 1:20,000). Total protein staining was performed for sample normalization (926-11016, Li-Cor). Antibody binding was visualized with an infrared imaging system (Odyssey, Li-Cor), and band quantification was performed with Image Studio 5.2.5 (Li-Cor).

Oxygen consumption measurement

Respiration rates were measured with Seahorse XFe96 Analyzer. Cardiomyocytes isolated from P14 to P21 mice were plated at ~2×10^4 cells per well of the 96-well XF96 Cell Culture Microplate (Agilent Technologies) and cultured for ~1 hour in Seahorse assay medium [pyruvate (0.55 mg/ml) in base medium, pH 7.4]. After determination of basal OCRs, cells were treated with oligomycin A (1 μM), carbonyl cyanide *p*-trifluoromethoxyphenylhydrazone (FCCP) (2 μM), and rotenone (1 μM) with antimycin A (1 μM). Cardiomyocyte numbers were counted and used to normalize the OCR.

ChIP analysis

DNA isolation for ChIP-qPCR analysis was performed using the protocol by van den Boogaard *et al.* (*74*). Briefly, several hearts (four to five hearts per sample) were isolated from P7 WT C57BL/6 mice and fixed in 1% paraformaldehyde followed by quenching with glycine. The heart tissue was subsequently homogenized and lysed using 1% SDS lysis buffer and protease inhibitor cocktail (Roche). DNA was fragmented using 20 cycles of 30 s "on" and then 30 s "off" of 50% power sonication, and DNA shearing efficiency was confirmed by DNA electrophoresis. Samples were subsequently incubated with protein G magnetic beads for 1 hour. Samples (2.5%) were kept as input (reference sample). Per2 ChIP-grade antibody (Novus, NB100-125) was added, and samples were incubated at 4°C overnight. Protein G magnetic beads were incubated for 1 hour and then pulled down. Chromatin was eluted from the beads and then uncrosslinked by incubating overnight at 65°C. DNA was purified using phenol-chloroform following ribonuclease A (RNase A) and proteinase K treatment (Thermo Fisher Scientific). DNA concentrations were calculated using the DNA Qubit 4 Fluorometer (Thermo Fisher Scientific). qPCR was performed using SYBR Select qPCR Mix (Thermo Fisher Scientific) with specific primers. Fold enrichment of DNA fragments compared to the input samples was calculated.

Heart norepinephrine measurement

P14 mouse hearts were harvested and placed in 0.01 N HCl with EDTA (1 mM) and sodium metabisulfite (4 mM) (pH > 7.0) to prevent norepinephrine degradation, and hearts were homogenized and stored at −80°C. Norepinephrine concentration was calculated using the Norepinephrine Elisa Kit (Abnova, KA3836) following the manufacturer's instructions.

Statistical analyses

All studies in cultured cells were performed using at least four sets of independent experiments. For in vivo studies, at least five animals in each group were analyzed. Student's *t* test was used for two-group analysis. Analysis of variance (ANOVA) with appropriate corrections for post hoc analysis was used for multiple group comparisons. *P* value of <0.05 was considered significant. Data were presented as means ± SEM. Graphs and statistical analysis were performed using GraphPad Prism V8. For RNA-sequencing analysis, Benjamini-Hochberg correction was used to adjust for multiple testing, with threshold of adjusted *P* value of <0.05 (i.e., false discovery rate < 10%) considered significant. For GO analysis, only pathways with *P* value of $<10^{-5}$ were reported.

Study approval

All protocols involving animals were approved by the animal and care use committee of the Johns Hopkins School of Medicine.

SUPPLEMENTARY MATERIALS

Supplementary material for this article is available at https://science.org/doi/10.1126/sciadv.abh4181

View/request a protocol for this paper from *Bio-protocol*.

REFERENCES AND NOTES

1. K. Fukuda, H. Kanazawa, Y. Aizawa, J. L. Ardell, K. Shivkumar, Cardiac innervation and sudden cardiac death. *Circ. Res.* **116**, 2005–2019 (2015).
2. A. M. D. Vegh, S. N. Duim, A. M. Smits, R. E. Poelmann, A. D. J. Ten Harkel, M. C. DeRuiter, M. J. Goumans, M. R. M. Jongbloed, Part and parcel of the cardiac autonomic nerve system: Unravelling its cellular building blocks during development. *J. Cardiovasc. Dev. Dis.* **3**, 28 (2016).
3. K. Kimura, M. Ieda, K. Fukuda, Development, maturation, and transdifferentiation of cardiac sympathetic nerves. *Circ. Res.* **110**, 325–336 (2012).
4. W. Hasan, Autonomic cardiac innervation:Development and adult plasticity. *Organogenesis* **9**, 176–193 (2013).
5. K. Haraldsdottir, A. M. Watson, K. N. Goss, A. G. Beshish, D. F. Pegelow, M. Palta, L. H. Tetri, G. P. Barton, M. D. Brix, R. M. Centanni, M. W. Eldridge, Impaired autonomic function in adolescents born preterm. *Physiol. Rep.* **6**, e13620 (2018).
6. A. J. Lewandowski, D. Augustine, P. Lamata, E. F. Davis, M. Lazdam, J. Francis, K. McCormick, A. R. Wilkinson, A. Singhal, A. Lucas, N. P. Smith, S. Neubauer, P. Leeson, Preterm heart in adult life: Cardiovascular magnetic resonance reveals distinct differences in left ventricular mass, geometry, and function. *Circulation* **127**, 197–206 (2013).
7. C. Crump, M. A. Winkleby, K. Sundquist, J. Sundquist, Risk of hypertension among young adults who were born preterm: A Swedish national study of 636,000 births. *Am. J. Epidemiol.* **173**, 797–803 (2011).
8. E. Tzahor, K. D. Poss, Cardiac regeneration strategies: Staying young at heart. *Science* **356**, 1035–1039 (2017).
9. E. R. Porrello, A. I. Mahmoud, E. Simpson, J. A. Hill, J. A. Richardson, E. N. Olson, H. A. Sadek, Transient regenerative potential of the neonatal mouse heart. *Science* **331**, 1078–1080 (2011).
10. M. H. Soonpaa, K. K. Kim, L. Pajak, M. Franklin, L. J. Field, Cardiomyocyte DNA synthesis and binucleation during murine development. *Am. J. Physiol.* **271**, H2183–H2189 (1996).
11. M. Hesse, A. Welz, B. K. Fleischmann, Heart regeneration and the cardiomyocyte cell cycle. *Pflugers Arch.* **470**, 241–248 (2018).
12. A. I. Mahmoud, F. Kocabas, S. A. Muralidhar, W. Kimura, A. S. Koura, S. Thet, E. R. Porrello, H. A. Sadek, Meis1 regulates postnatal cardiomyocyte cell cycle arrest. *Nature* **497**, 249–253 (2013).
13. T. Heallen, M. Zhang, J. Wang, M. Bonilla-Claudio, E. Klysik, R. L. Johnson, J. F. Martin, Hippo pathway inhibits Wnt signaling to restrain cardiomyocyte proliferation and heart size. *Science* **332**, 458–461 (2011).
14. A. Eulalio, M. Mano, M. Dal Ferro, L. Zentilin, G. Sinagra, S. Zacchigna, M. Giacca, Functional screening identifies miRNAs inducing cardiac regeneration. *Nature* **492**, 376–381 (2012).
15. T. M. A. Mohamed, Y. S. Ang, E. Radzinsky, P. Zhou, Y. Huang, A. Elfenbein, A. Foley, S. Magnitsky, D. Srivastava, Regulation of cell cycle to stimulate adult cardiomyocyte proliferation and cardiac regeneration. *Cell* **173**, 104–116.e12 (2018).
16. H. Liu, C. H. Zhang, N. Ammanamanchi, S. Suresh, C. Lewarchik, K. Rao, G. M. Uys, L. Han, M. Abrial, D. Yimlamai, B. Ganapathy, C. Guillermier, N. Chen, M. Khaladkar, J. Spaethling, J. H. Eberwine, J. Kim, S. Walsh, S. Choudhury, K. Little, K. Francis, M. Sharma, M. Viegas, A. Bais, D. Kostka, J. Ding, Z. Bar-Joseph, Y. Wu, V. Yechoor, M. Moulik, J. Johnson, J. Weinberg, M. Reyes-Mugica, M. L. Steinhauser, B. Kuhn, Control of cytokinesis by beta-adrenergic receptors indicates an approach for regulating cardiomyocyte endowment. *Sci. Transl. Med.* **11**, eaaw6419 (2019).
17. R. E. Kreipke, S. J. Birren, Innervating sympathetic neurons regulate heart size and the timing of cardiomyocyte cell cycle withdrawal. *J. Physiol.* **593**, 5057–5073 (2015).
18. J. D. Kugler, P. C. Gillette, S. P. Graham, A. Garson Jr., M. A. Goldstein, H. K. Thompson Jr., Effect of chemical sympathectomy on myocardial cell division in the newborn rat. *Pediatr. Res.* **14**, 881–884 (1980).
19. V. Bagga, S. B. Dunnett, R. A. Fricker, The 6-OHDA mouse model of Parkinson's disease - Terminal striatal lesions provide a superior measure of neuronal loss and replacement than median forebrain bundle lesions. *Behav. Brain Res.* **288**, 107–117 (2015).
20. A. I. Mahmoud, C. C. O'Meara, M. Gemberling, L. Zhao, D. M. Bryant, R. Zheng, J. B. Gannon, L. Cai, W. Y. Choi, G. F. Egnaczyk, C. E. Burns, C. G. Burns, C. A. MacRae, K. D. Poss, R. T. Lee, Nerves regulate cardiomyocyte proliferation and heart regeneration. *Dev. Cell* **34**, 387–399 (2015).
21. I. A. White, J. Gordon, W. Balkan, J. M. Hare, Sympathetic reinnervation is required for mammalian cardiac regeneration. *Circ. Res.* **117**, 990–994 (2015).

22. J. Nam, I. Onitsuka, J. Hatch, Y. Uchida, S. Ray, S. Huang, W. Li, H. Zang, P. Ruiz-Lozano, Y. S. Mukouyama, Coronary veins determine the pattern of sympathetic innervation in the developing heart. *Development* **140**, 1475–1485 (2013).
23. Y. Guo, W. T. Pu, Cardiomyocyte maturation: New phase in development. *Circ. Res.* **126**, 1086–1106 (2020).
24. E. Karbassi, A. Fenix, S. Marchiano, N. Muraoka, K. Nakamura, X. Yang, C. E. Murry, Cardiomyocyte maturation: Advances in knowledge and implications for regenerative medicine. *Nat. Rev. Cardiol.* **17**, 341–359 (2020).
25. N. O. Glebova, D. D. Ginty, Heterogeneous requirement of NGF for sympathetic target innervation in vivo. *J. Neurosci.* **24**, 743–751 (2004).
26. Z. Zhou, J. Wang, C. Guo, W. Chang, J. Zhuang, P. Zhu, X. Li, Temporally distinct Six2-positive second heart field progenitors regulate mammalian heart development and disease. *Cell Rep.* **18**, 1019–1032 (2017).
27. X. Jiang, D. H. Rowitch, P. Soriano, A. P. McMahon, H. M. Sucov, Fate of the mammalian cardiac neural crest. *Development* **127**, 1607–1616 (2000).
28. A. Shostak, Circadian clock, cell division, and cancer: From molecules to organism. *Int. J. Mol. Sci.* **18**, (2017).
29. J. Gaucher, E. Montellier, P. Sassone-Corsi, Molecular cogs: Interplay between circadian clock and cell cycle. *Trends Cell Biol.* **28**, 368–379 (2018).
30. T. Matsuo, S. Yamaguchi, S. Mitsui, A. Emi, F. Shimoda, H. Okamura, Control mechanism of the circadian clock for timing of cell division in vivo. *Science* **302**, 255–259 (2003).
31. C. Feillet, G. T. van der Horst, F. Levi, D. A. Rand, F. Delaunay, Coupling between the circadian clock and cell cycle oscillators: Implication for healthy cells and malignant growth. *Front. Neurol.* **6**, 96 (2015).
32. A. A. Shafi, K. E. Knudsen, Cancer and the circadian clock. *Cancer Res.* **79**, 3806–3814 (2019).
33. S. Lee, L. A. Donehower, A. J. Herron, D. D. Moore, L. Fu, Disrupting circadian homeostasis of sympathetic signaling promotes tumor development in mice. *PLOS ONE* **5**, e10995 (2010).
34. J. S. Takahashi, Transcriptional architecture of the mammalian circadian clock. *Nat. Rev. Genet.* **18**, 164–179 (2017).
35. S. Gery, N. Komatsu, L. Baldjyan, A. Yu, D. Koo, H. P. Koeffler, The circadian gene per1 plays an important role in cell growth and DNA damage control in human cancer cells. *Mol. Cell* **22**, 375–382 (2006).
36. E. Kowalska, J. A. Ripperger, D. C. Hoegger, P. Bruegger, T. Buch, T. Birchler, A. Mueller, U. Albrecht, C. Contaldo, S. A. Brown, NONO couples the circadian clock to the cell cycle. *Proc. Natl. Acad. Sci. U.S.A.* **110**, 1592–1599 (2013).
37. L. Fu, M. S. Patel, A. Bradley, E. F. Wagner, G. Karsenty, The molecular clock mediates leptin-regulated bone formation. *Cell* **122**, 803–815 (2005).
38. H. Terazono, T. Mutoh, S. Yamaguchi, M. Kobayashi, M. Akiyama, R. Udo, S. Ohdo, H. Okamura, S. Shibata, Adrenergic regulation of clock gene expression in mouse liver. *Proc. Natl. Acad. Sci. U.S.A.* **100**, 6795–6800 (2003).
39. S. Beesley, T. Noguchi, D. K. Welsh, Cardiomyocyte circadian oscillations are cell-autonomous, amplified by β-adrenergic signaling, and synchronized in cardiac ventricle tissue. *PLOS ONE* **11**, e0159618 (2016).
40. S. A. Tischkau, J. W. Mitchell, S. H. Tyan, G. F. Buchanan, M. U. Gillette, Ca2+/cAMP response element-binding protein (CREB)-dependent activation of Per1 is required for light-induced signaling in the suprachiasmatic nucleus circadian clock. *J. Biol. Chem.* **278**, 718–723 (2003).
41. J. Y. Altarejos, M. Montminy, CREB and the CRTC co-activators: Sensors for hormonal and metabolic signals. *Nat. Rev. Mol. Cell Biol.* **12**, 141–151 (2011).
42. B. C. du Pre, P. Dierickx, S. Crnko, P. A. Doevendans, M. A. Vos, N. Geijsen, D. Neutel, T. A. B. van Veen, L. W. van Laake, Neonatal rat cardiomyocytes as an in vitro model for circadian rhythms in the heart. *J. Mol. Cell. Cardiol.* **112**, 58–63 (2017).
43. S. D. Williams, H. Zhu, L. Zhang, H. S. Bernstein, Adenoviral delivery of human CDC5 promotes G2/M progression and cell division in neonatal ventricular cardiomyocytes. *Gene Ther.* **13**, 837–843 (2006).
44. F. C. Kelleher, A. Rao, A. Maguire, Circadian molecular clocks and cancer. *Cancer Lett.* **342**, 9–18 (2014).
45. A. C. Cardoso, N. T. Lam, J. J. Savla, Y. Nakada, A. H. M. Pereira, A. Elnwasany, I. Menendez-Montes, E. L. Ensley, U. B. Petric, G. Sharma, A. D. Sherry, C. R. Malloy, C. Khemtong, M. T. Kinter, W. L. W. Tan, C. G. Anene-Nzelu, R. S. Foo, N. U. N. Nguyen, S. Li, M. S. Ahmed, W. M. Elhelaly, S. Abdisalaam, A. Asaithamby, C. Xing, M. Kanchwala, G. Vale, K. M. Eckert, M. A. Mitsche, J. G. McDonald, J. A. Hill, L. Huang, P. W. Shaul, L. I. Szweda, H. A. Sadek, Mitochondrial substrate utilization regulates cardiomyocyte cell cycle progression. *Nat. Metab.* **2**, 167–178 (2020).
46. N. Koike, S. H. Yoo, H. C. Huang, V. Kumar, C. Lee, T. K. Kim, J. S. Takahashi, Transcriptional architecture and chromatin landscape of the core circadian clock in mammals. *Science* **338**, 349–354 (2012).
47. S. Ogawa, J. V. Barnett, L. Sen, J. B. Galper, T. W. Smith, J. D. Marsh, Direct contact between sympathetic neurons and rat cardiac myocytes in vitro increases expression of functional calcium channels. *J. Clin. Invest.* **89**, 1085–1093 (1992).
48. J. Qu, R. B. Robinson, Cardiac ion channel expression and regulation: The role of innervation. *J. Mol. Cell. Cardiol.* **37**, 439–448 (2004).
49. Y. Oh, G. S. Cho, Z. Li, I. Hong, R. Zhu, M. J. Kim, Y. J. Kim, E. Tampakakis, L. Tung, R. Huganir, X. Dong, C. Kwon, G. Lee, Functional coupling with cardiac muscle promotes maturation of hPSC-derived sympathetic neurons. *Cell Stem Cell* **19**, 95–106 (2016).
50. Y. T. Tseng, R. Kopel, J. P. Stabila, B. G. McGonnigal, T. T. Nguyen, P. A. Gruppuso, J. F. Padbury, Beta-adrenergic receptors (ßAR) regulate cardiomyocyte proliferation during early postnatal life. *FASEB J.* **15**, 1921–1926 (2001).
51. S. Engelhardt, L. Hein, F. Wiesmann, M. J. Lohse, Progressive hypertrophy and heart failure in beta1-adrenergic receptor transgenic mice. *Proc. Natl. Acad. Sci. U.S.A.* **96**, 7059–7064 (1999).
52. R. Wadhawan, Y. T. Tseng, J. Stabila, B. McGonnigal, S. Sarkar, J. Padbury, Regulation of cardiac beta 1-adrenergic receptor transcription during the developmental transition. *Am. J. Physiol. Heart Circ. Physiol.* **284**, H2146–H2152 (2003).
53. A. Ikenishi, H. Okayama, N. Iwamoto, S. Yoshitome, S. Tane, K. Nakamura, T. Obayashi, T. Hayashi, T. Takeuchi, Cell cycle regulation in mouse heart during embryonic and postnatal stages. *Dev. Growth Differ.* **54**, 731–738 (2012).
54. B. N. Puente, W. Kimura, S. A. Muralidhar, J. Moon, J. F. Amatruda, K. L. Phelps, D. Grinsfelder, B. A. Rothermel, R. Chen, J. A. Garcia, C. X. Santos, S. Thet, E. Mori, M. T. Kinter, P. M. Rindler, S. Zacchigna, S. Mukherjee, D. J. Chen, A. I. Mahmoud, M. Giacca, P. S. Rabinovitch, A. Aroumougame, A. M. Shah, L. I. Szweda, H. A. Sadek, The oxygen-rich postnatal environment induces cardiomyocyte cell-cycle arrest through DNA damage response. *Cell* **157**, 565–579 (2014).
55. Y. Umemura, N. Koike, M. Ohashi, Y. Tsuchiya, Q. J. Meng, Y. Minami, M. Hara, M. Hisatomi, K. Yagita, Involvement of posttranscriptional regulation of Clock in the emergence of circadian clock oscillation during mouse development. *Proc. Natl. Acad. Sci. U.S.A.* **114**, E7479–E7488 (2017).
56. M. S. Bray, C. A. Shaw, M. W. Moore, R. A. Garcia, M. M. Zanquetta, D. J. Durgan, W. J. Jeong, J. Y. Tsai, H. Bugger, D. Zhang, A. Rohrwasser, J. H. Rennison, J. R. Dyck, S. E. Litwin, P. E. Hardin, C. W. Chow, M. P. Chandler, E. D. Abel, M. E. Young, Disruption of the circadian clock within the cardiomyocyte influences myocardial contractile function, metabolism, and gene expression. *Am. J. Physiol. Heart Circ. Physiol.* **294**, H1036–H1047 (2008).
57. T. A. Martino, M. E. Young, Influence of the cardiomyocyte circadian clock on cardiac physiology and pathophysiology. *J. Biol. Rhythms* **30**, 183–205 (2015).
58. J. Hirayama, L. Cardone, M. Doi, P. Sassone-Corsi, Common pathways in circadian and cell cycle clocks: Light-dependent activation of Fos/AP-1 in zebrafish controls CRY-1a and WEE-1. *Proc. Natl. Acad. Sci. U.S.A.* **102**, 10194–10199 (2005).
59. Y. Han, F. Meng, J. Venter, N. Wu, Y. Wan, H. Standeford, H. Francis, C. Meininger, J. Greene Jr., J. P. Trzeciakowski, L. Ehrlich, S. Glaser, G. Alpini, miR-34a-dependent overexpression of Per1 decreases cholangiocarcinoma growth. *J. Hepatol.* **64**, 1295–1304 (2016).
60. X. J. Fu, H. X. Li, K. Yang, D. Chen, H. Tang, The important tumor suppressor role of PER1 in regulating the cyclin-CDK-CKI network in SCC15 human oral squamous cell carcinoma cells. *Onco. Targets Ther.* **9**, 2237–2245 (2016).
61. S. A. Huisman, A. R. Ahmadi, J. N. M. IJzermans, C. Verhoef, G. T. van der Horst, R. W. de Bruin, Disruption of clock gene expression in human colorectal liver metastases. *Tumour Biol.* **37**, 13973–13981 (2016).
62. W. Yu, M. Nomura, M. Ikeda, Interactivating feedback loops within the mammalian clock: BMAL1 is negatively autoregulated and upregulated by CRY1, CRY2, and PER2. *Biochem. Biophys. Res. Commun.* **290**, 933–941 (2002).
63. R. El Cheikh, S. Bernard, N. El Khatib, Modeling circadian clock-cell cycle interaction effects on cell population growth rates. *J. Theor. Biol.* **363**, 318–331 (2014).
64. E. Tampakakis, A. I. Mahmoud, The role of hormones and neurons in cardiomyocyte maturation. *Semin. Cell Dev. Biol.* **118**, 136–143 (2021).
65. H. Uosaki, P. Cahan, D. I. Lee, S. Wang, M. Miyamoto, L. Fernandez, D. A. Kass, C. Kwon, Transcriptional landscape of cardiomyocyte maturation. *Cell Rep.* **13**, 1705–1716 (2015).
66. S. A. Murphy, E. Z. Chen, L. Tung, K. R. Boheler, C. Kwon, Maturing heart muscle cells: Mechanisms and transcriptomic insights. *Semin. Cell Dev. Biol.* **119**, 49–60 (2021).
67. M. A. Wheeler, D. L. Heffner, S. Kim, S. M. Espy, A. J. Spano, C. L. Cleland, C. D. Deppmann, TNF-α/TNFR1 signaling is required for the development and function of primary nociceptors. *Neuron* **82**, 587–602 (2014).
68. M. Muller, V. Triaca, D. Besusso, M. Costanzi, J. M. Horn, J. Koudelka, M. Geibel, V. Cestari, L. Minichiello, Loss of NGF-TrkA signaling from the CNS is not sufficient to induce cognitive impairments in young adult or intermediate-aged mice. *J. Neurosci.* **32**, 14885–14898 (2012).
69. Y. Saga, S. Miyagawa-Tomita, A. Takagi, S. Kitajima, J. Miyazaki, T. Inoue, MesP1 is expressed in the heart precursor cells and required for the formation of a single heart tube. *Development* **126**, 3437–3447 (1999).
70. G. S. Cho, D. I. Lee, E. Tampakakis, S. Murphy, P. Andersen, H. Uosaki, S. Chelko, K. Chakir, I. Hong, K. Seo, H. V. Chen, X. Chen, C. Basso, S. R. Houser, G. F. Tomaselli, B. O'Rourke,

D. P. Judge, D. A. Kass, C. Kwon, Neonatal transplantation confers maturation of PSC-derived cardiomyocytes conducive to modeling cardiomyopathy. *Cell Rep.* **18**, 571–582 (2017).
71. M. Stahlberg, R. Nakagawa, D. Bedja, G. Zhu, B. L. Lin, A. Saberi, D. I. Lee, D. A. Kass, Chronic atrial and ventricular pacing in the mouse. *Circ. Heart Fail.* **12**, e005655 (2019).
72. J. Thireau, B. L. Zhang, D. Poisson, D. Babuty, Heart rate variability in mice: A theoretical and practical guide. *Exp. Physiol.* **93**, 83–94 (2008).
73. A. M. Bolger, M. Lohse, B. Usadel, Trimmomatic: A flexible trimmer for Illumina sequence data. *Bioinformatics* **30**, 2114–2120 (2014).
74. M. van den Boogaard, L. Y. Wong, V. M. Christoffels, P. Barnett, Acquisition of high quality DNA for massive parallel sequencing by in vivo chromatin immunoprecipitation. *Methods Mol. Biol.* **977**, 53–64 (2013).

Acknowledgments: We thank Kwon laboratory members for critical reading and discussions. We also thank M. Stahlberg and R. Nakagawa for assistance with mouse ECG recordings, M. Ranek for assistance with Western blotting, and R. Kuruvilla for helpful suggestions.

Funding: E.T. is supported by NHLBI (HL-145135), AHA (CDA34660077), W.W. Smith Charitable Trust, and the Magic that Matters Fund. C.K. is supported by NIH (R01HL156947 and 1R01HD086026), AHA (18EIA3389003), MSCRF (2019-MSCRFD-5044), and JHU Mirowski Award.
Author contributions: E.T. designed, carried out, and supervised this work and wrote the manuscript. H.G., M.H., and S.G. assisted with experimental work. S.M. performed bioinformatics analyses and assisted with ChIP analysis. B.L.L. assisted with cell isolation. A.S. performed bioinformatics analyses. M.M. assisted with cell analysis. T.L. assisted with Seahorse analyses. W.K., Y.-S.M., G.L., and L.M. assisted with experimental design. C.K. supervised this work and wrote the manuscript. **Competing interests:** The authors declare that they have no competing interests. **Data and materials availability:** All data needed to evaluate the conclusions in the paper are present in the paper and/or the Supplementary Materials.

Submitted 8 March 2021
Accepted 8 October 2021
Published 1 December 2021
10.1126/sciadv.abh4181